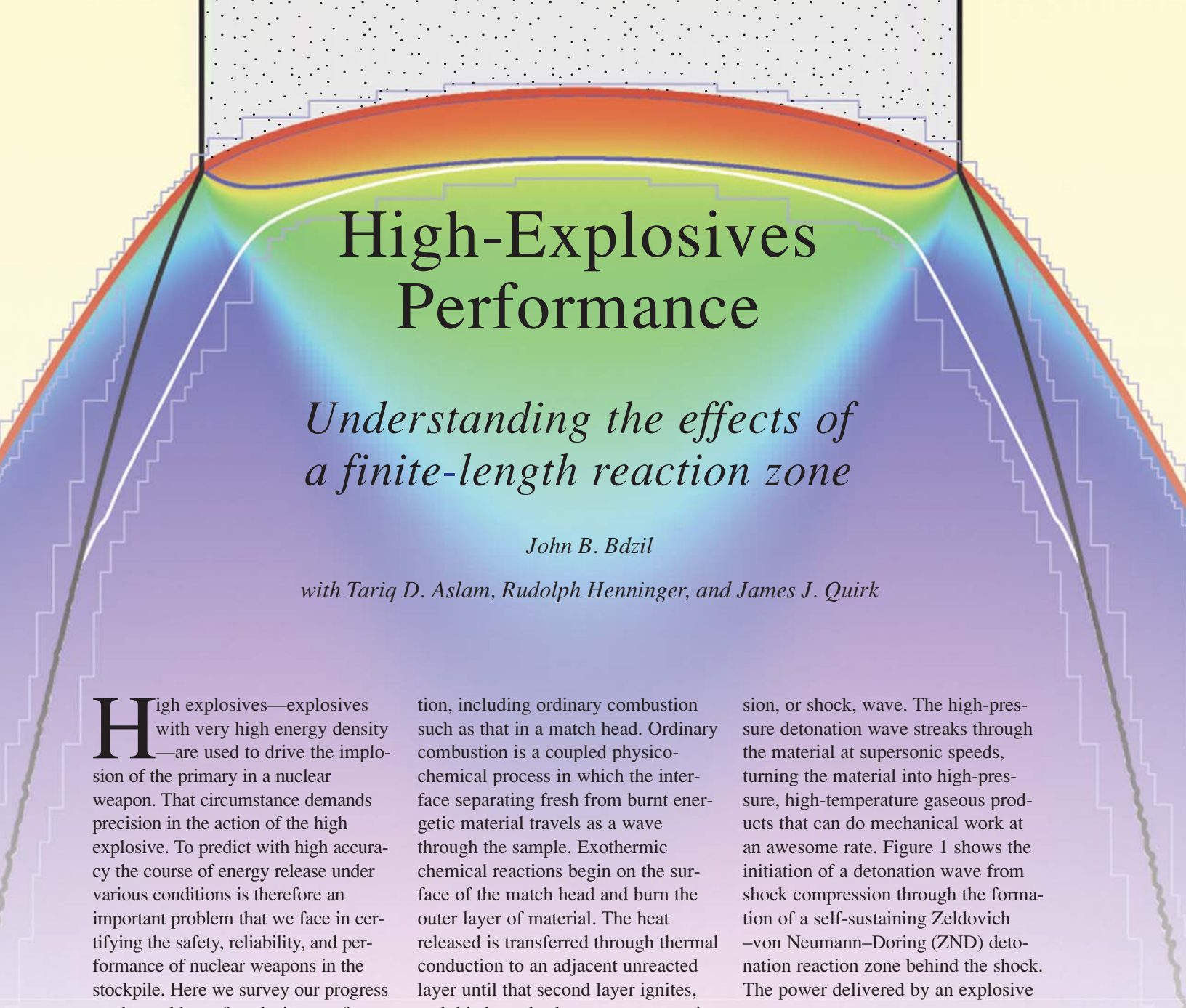

High-Explosives Performance

Understanding the effects of a finite-length reaction zone

John B. Bdzil

with Tariq D. Aslam, Rudolph Henninger, and James J. Quirk

High explosives—explosives with very high energy density—are used to drive the implosion of the primary in a nuclear weapon. That circumstance demands precision in the action of the high explosive. To predict with high accuracy the course of energy release under various conditions is therefore an important problem that we face in certifying the safety, reliability, and performance of nuclear weapons in the stockpile. Here we survey our progress on the problem of explosives performance: predicting the outcome of intentional detonation of high explosives in complex three-dimensional (3-D) geometries. The problems of safety (accidental initiation) and reliability (reproducible response to a prescribed stimulus) are also under investigation but will be only briefly mentioned here.

Explosives belong to the class of combustibles known as energetic materials, which means that they contain both fuel and oxidizer premixed on a molecular level. Such materials can support a whole range of combustion, including ordinary combustion such as that in a match head. Ordinary combustion is a coupled physicochemical process in which the interface separating fresh from burnt energetic material travels as a wave through the sample. Exothermic chemical reactions begin on the surface of the match head and burn the outer layer of material. The heat released is transferred through thermal conduction to an adjacent unreacted layer until that second layer ignites, and this layer-by-layer process continues until the entire sample is consumed. The speed of the combustion wave is relatively low, depending on both the rate of energy transport from one layer to the next and the rate of the local exothermic chemical reactions in each layer.

Explosives, in contrast, support very high speed combustion known as detonation. Like an ordinary combustion wave, a detonation wave derives its energy from the chemical reactions in the material, but the energy transport occurs not by thermal conduction but rather by a high-speed compression, or shock, wave. The high-pressure detonation wave streaks through the material at supersonic speeds, turning the material into high-pressure, high-temperature gaseous products that can do mechanical work at an awesome rate. Figure 1 shows the initiation of a detonation wave from shock compression through the formation of a self-sustaining Zeldovich –von Neumann–Doring (ZND) detonation reaction zone behind the shock. The power delivered by an explosive

The pressure plot on this opening page shows a steady-state detonation wave propagating through a cylindrical explosive (gray) confined by a low-density inert material (yellow). Red is the highest pressure; purple, the lowest. The reaction starts along the shock (red curve) and ends along the sonic surface (white curve). A large pressure drop at the edge of the explosive leads to a significant lengthening of the chemical reaction zone near the edges of the detonating explosive, a reduction in the speed of the detonation wave, and the development of a curved detonation shock front.

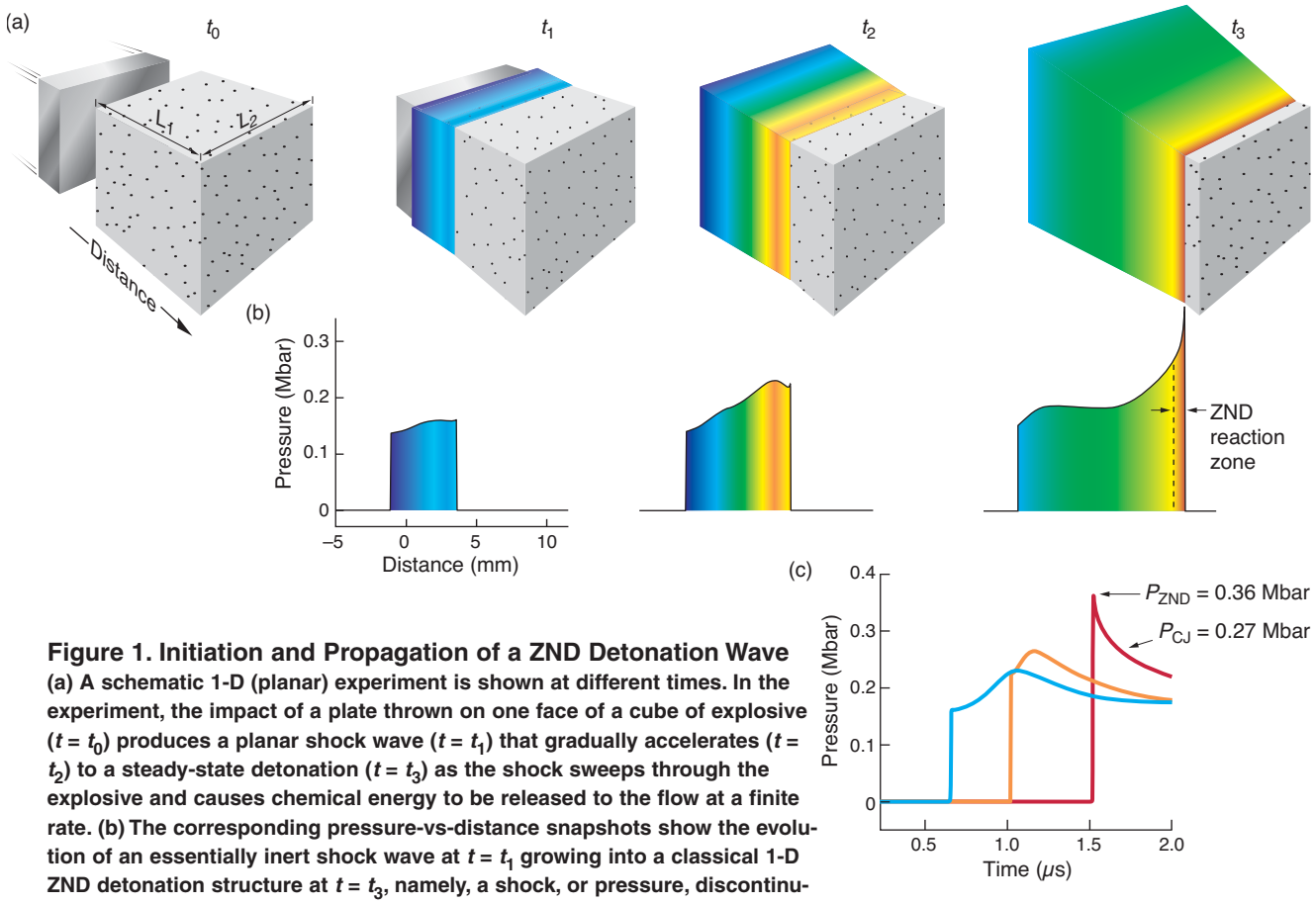

Figure 1. Initiation and Propagation of a ZND Detonation Wave
(a) A schematic 1-D (planar) experiment is shown at different times. In the experiment, the impact of a plate thrown on one face of a cube of explosive ($t = t_0$) produces a planar shock wave ($t = t_1$) that gradually accelerates ($t = t_2$) to a steady-state detonation ($t = t_3$) as the shock sweeps through the explosive and causes chemical energy to be released to the flow at a finite rate. (b) The corresponding pressure-vs-distance snapshots show the evolution of an essentially inert shock wave at $t = t_1$ growing into a classical 1-D ZND detonation structure at $t = t_3$, namely, a shock, or pressure, discontinuity at the ZND point followed by decreasing pressure through the reaction zone, ending at the CJ point, the pressure predicted by the simple CJ model (see text). (c) Pressure-vs-time plots for material particles originally at the shock front locations in (b) show the particle pressure (or velocity) histories in the form measured in actual experiments (see Figures 5, 6, and 7). Only at the location of the rightmost particle has a ZND detonation fully formed. Note: The point of maximum acceleration of the shock, called the point of detonation formation, coincides with the shape change in the pressure profile and the first appearance of a choked flow condition (sonic condition). Refer to Figure 3.

depends on its energy density and its detonation wave speed. Solid high explosives, like those used in nuclear weapons, have a detonation speed of about 8000 meters per second (m/s), or three times the speed of sound in the explosive, a high liberated energy density of about 5 megajoules per kilogram (MJ/kg), and an initial material density of about 2000 kilograms per cubic meter (kg/m^3). The product of these three quantities yields the enormous power density of 80,000,000 MJ/m^2/s or 8×10^9 watts per centimeter squared (W/cm^2). By comparison, a detonation with a surface area of 100 centimeters squared operates at a power level equal to the total electric generating capacity of the United States! This very rapid rate of energy liberation is what makes solid explosives unique and useful.

The legacy weapons codes have long used the simple Chapman-Jouguet (CJ) model to compute the performance of high explosives. In this classical, one-dimensional (1-D) model of detonation, it is assumed that the chemical reaction rate is infinite (and therefore the length of the reaction zone is zero rather than finite, as in the opening figure and Figure 1). That assumption leads to the prediction that the detonation speed is constant. Moreover, the values of the detonation speed, D_{CJ}, as well as the detonation pressure, P_{CJ}, are independent of the initiating shock strength and depend on only certain properties of the explosive before and after passage of the detonation front, namely, the initial density of the unreacted material, the liberated energy density of the explosive, and the pressure–volume (P-v) response function of the reacted material (called the mechanical equation of state, or EOS). In this CJ limit, the explosive performance problem is reduced to providing an accurate mechanical EOS for the gaseous products of detonation, E_g (P,v)—see Figure 2.

In this article, we focus on another aspect of the performance problem:

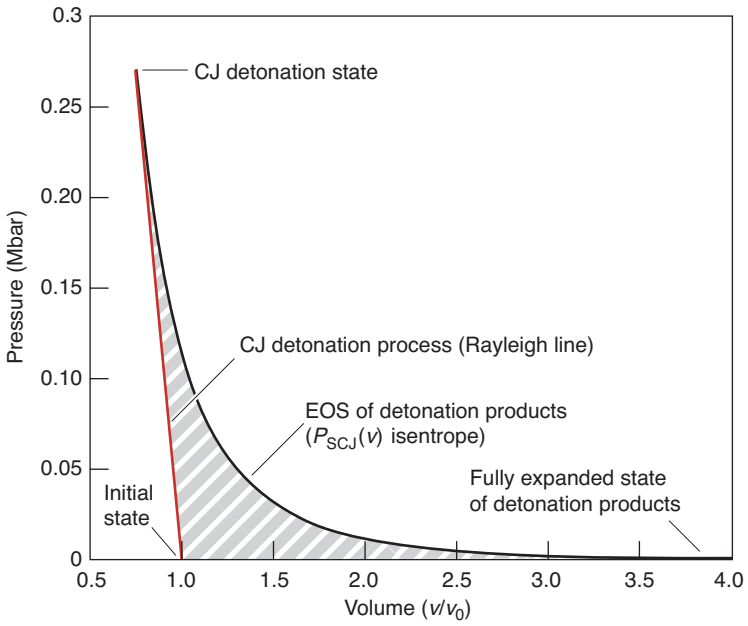

Figure 2. Maximum Work Obtainable from a CJ Detonation

The $E_g(P, v)$ mechanical equation of state (EOS) is required to model explosive performance. Most often, it is measured along a restricted curve—an isentrope, $P_S(v)$, or a shock Hugoniot curve, $P_H(v)$—in the state space defined by the thermodynamic variables E_g, P, and v. To characterize the maximum work that a detonation can perform (shaded area above), we need determine only the principal or CJ expansion isentrope of the detonation products, $P_{SCJ}(v)$, given that we know D_{CJ}, and P_{CJ}. The two curves shown above are the detonation Rayleigh line, shown in red (detonation process), and the detonation products expansion isentrope, $P_{SCJ}(v)$. The area under the isentrope (to some cut-off pressure) minus the area under the Rayleigh line (work done by the shock in compressing the explosive) is the maximum mechanical work that can be obtained from the explosive. For our high-performance, monomolecular explosives, such as HMX, this work compared with the available explosive energy can be very high (more than 90%). We perform experiments to measure this isentrope and then construct the $E_g(P, v)$ mechanical EOS for the products of detonation, which is an essential ingredient in every model of how detonations do work on their surroundings. We are working on both better theoretical (Shaw 2002) and experimental (Hill 2002) methods for determining the $E_g(P, v)$ EOS.

creating accurate 3-D detonation models that account for the effects of finite chemical reaction rates (and therefore a finite reaction-zone length behind the detonation front). The finite length of the reaction zone has many effects. For example, it can affect the detonation speed and therefore the power level at which a detonation engine operates on inert materials. It also places limits on the minimum size of the explosive and the minimum input pressure that will lead to detonation, especially in geometries that cause detonation waves to go around corners, say, near a small detonator. The models we have been developing are specifically designed for adaptation to the legacy codes and to the Advanced Simulation and Computing (ASCI) high-fidelity codes used to study weapons performance. Known as detonation shock dynamics (DSD), these are subscale (or subgrid) models that capture the physics of the reaction zone without explicitly modeling that zone and, therefore, without requiring enormous computing time. Although they are state of the art for modeling 3-D detonation flows, our models predict detonation propagation only in homogeneous explosives under standard conditions. That is, they do not fully account for the effects that the heterogeneity of the real explosives we use today have on detonation. We therefore conclude this article with our vision for the future of detonation propagation modeling—one that accounts for that heterogeneity yet remains practical for weapons performance studies.

The Detonation Process

How does a detonation wave reach and then maintain such enormous power levels as it sweeps through the explosive? The enormous pressures (a few hundred thousand atmospheres, or a few hundred kilobars) and temperatures (2000 to 4000 kelvins) behind the detonation front originate from the very rapid release of chemical energy. Reactions are 90 percent complete in less than a millionth of a second. As a result of this rapid release, the reaction zone is very short. But how are the pressures sustained?

As shown in Figure 3, the reaction zone is bounded by two surfaces that isolate it from the regions ahead and behind it and thereby maintain its extreme pressure. First is the shock surface, which initiates the reaction. Because it travels at supersonic speed relative to the unreacted material, it prevents any leakage of pressure ahead of the shock. Second is the sonic surface (labeled choked-flow state), which moves at the local speed of sound in the frame of the moving shock front. To explain the effect of this surface, we consider an observer riding with the shock and looking back. The observer sees an increasing amount of energy release back into the reaction zone as a func-

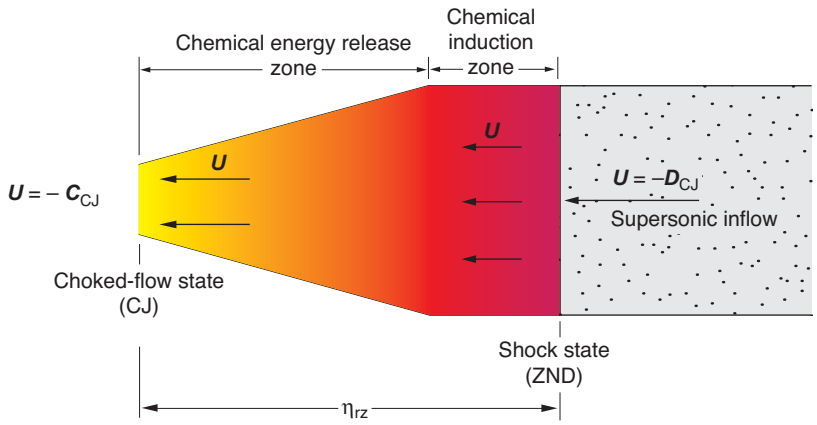

Figure 3. The Finite-Length, Self-Sustaining Reaction Zone
In many respects, the self-sustaining detonation reaction zone operates like a rocket motor. The reaction zone is bounded by the shock surface at the detonation front and the choked flow-state surface some distance behind. Those two surfaces isolate the reaction zone from the regions in front of it and behind it and thereby maintain its extreme pressure. Looking backward in the frame that moves with the detonation shock front, one observes that an increasing amount of heat added to the flow with increasing distance into the reaction zone acts like a nozzle in a rocket, accelerating the flow to sonic speeds, C_{CJ}.

tion of distance. This energy release serves to accelerate the flow away from the shock front and reduce the pressure, in much the same way as a rocket nozzle accelerates the gas ejected from a rocket and thereby propels the rocket forward. As the reaction is completed, the flow speed at the end of the reaction zone becomes equal to the local speed of sound in the frame moving with the shock, C_{CJ}. As a result, the flow becomes choked and thereby stops any further pressure decrease in the reaction zone. Collectively, these two effects are referred to as inertial confinement.

Another way to understand inertial confinement at the sonic surface is to note that the postreaction-zone flow (left of the sonic surface) in the reference frame of the shock is supersonic. Consequently, the reaction zone is essentially isolated from disturbances originating in the flow behind it. Insulated from its surroundings, detonation is self-propagating, depending only on what is happening in the reaction zone.

Real vs Idealized Explosives

If an explosive is to be useful in engineering applications—be they mining, nuclear weapons, or modern "smart" munitions—its chemical reaction rate must be essentially zero at the ambient state and must become extremely fast once passage of a shock wave substantially increases the pressure and temperature in the material. As mentioned above, in the classical CJ model, the chemical reaction rate after the shock front has passed is infinite, the reaction-zone length goes to zero, and the detonation wave travels through the material at a constant speed and pressure. In reality, the explosives we use in practical applications do not behave like the ideal CJ model but have finite reaction rates. This situation is indeed fortunate. If the reaction rate were infinite and the reaction zone of length zero, then subjecting even a tiny region of the explosive to a high pressure or high temperature would initiate detonation of the entire sample. The extreme sensitivity of explosives such as nitroglycerine is legendary in this regard.

Because the reaction rate and reaction-zone length of practical explosives depend significantly on pressure and temperature, a sample subjected to a weak initial shock will experience transients during initiation of detonation. If the sample is a slab of finite thickness (L_1 in Figure 1) but infinite lateral extent ($L_2 \to \infty$), the shock can pass through the slab in a short time compared with the duration of the transient, and no detonation occurs. Conversely, to initiate detonation in a sample of finite thickness with finite reaction-zone length, the shock must have a finite strength. That decrease in sensitivity caused by a finite reaction-zone length is what makes practical explosives safe enough to handle.

The fact that real explosive samples have a finite lateral extent (L_2 in Figure 1) also contributes to reducing sensitivity. Some of the energy released in the reaction zone leaks out of the sides of the explosive transverse to the direction of detonation propagation and thereby reduces the support for the forward motion of the shock. If that energy loss is too great, detonation dies out. Thus, the longer the reaction zone in practical explosives, the more difficult they are to detonate—or, in other words, the more insensitive (and safer) they are.

One way to control sensitivity is to control the "effective," or global, reaction rate as opposed to the local reaction rates. Alfred Nobel used this technique to turn the liquid explosive nitroglycerine into dynamite. Nitroglycerine is an extremely sensitive explosive because its high viscosity allows it to form bubbles easily. When these bubbles collapse, they generate localized high pressures and temperatures called hotspots. The hotspots serve as initiation sites for localized, rapid reaction, leading to the establishment of

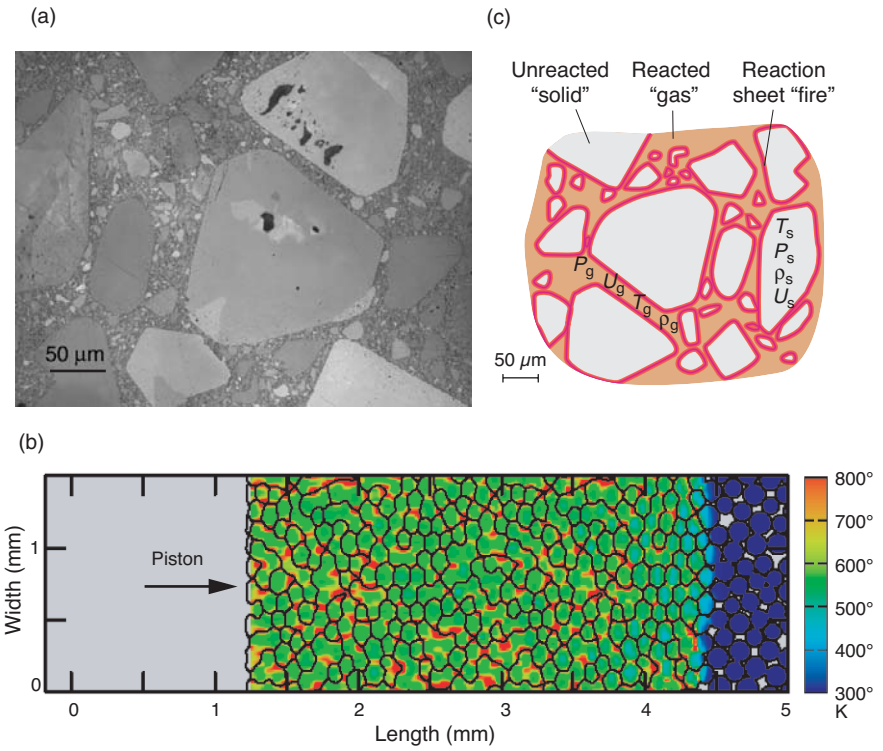

Figure 4. Substructure of Heterogeneous High Explosives
(a) The photomicrograph shows the granular substructure of PBX 9501 (Skidmore et al. 1998). (b) A numerical simulation shows the temperature distribution that develops in a heterogeneous material subjected to rapid, compressive loading (Menikoff and Kober 1999). (c) The drawing shows a detailed view of the hotspots that develop when explosives such as PBX 9501 are subjected to a shock wave. We are not yet able to accurately model such complex, micromechanical hydrodynamic interactions.

localized detonation that spreads through the otherwise cool material and consumes it all. By adding a highly porous silica to nitroglycerine, Nobel turned the material into a paste, thereby suppressing small bubble formation and dramatically reducing its sensitivity.

At Los Alamos, we have followed the reverse path. We start from a very insensitive explosive and increase its sensitivity by using it in the form of small granules that serve as centers for initiation of chemical reaction hotspots and subsequent detonation. A typical example of these insensitive, high-mass, high-energy-density solid explosives is HMX. To detonate a single crystal of this material, a few centimeters on a side and free of most physical defects, requires an input shock pressure of hundreds of kilobars (Campbell and Travis 1985). To increase the effective, average global reaction rate, we formulate a mixture of small, heterogeneous HMX granules and polymeric binder and then press the mixture to a density approaching that of pure, crystalline HMX. By controlling the size of the granules and the final pressed density, we can vary the sensitivity of the explosive. The granular HMX explosive PBX 9501 requires only tens of kilobars of pressure to initiate detonation within a fraction of a centimeter.

Despite our control over the manufacturing and thus the reproducibility of explosive detonation, we cannot predict the effective reaction rates in such heterogeneous HMX explosives from first principles. One reason is that we have been unable to measure the chemical route by which the solid explosives decompose to gaseous products under the extreme conditions of detonation (about 0.5 megabar in pressure at temperatures of 3000 kelvins). Only recently did we acquire appropriate techniques to address those questions. In particular, we can now generate and characterize planar shocks using a combination of ultrafast lasers and interferometers. In the future, we hope to use ultrafast laser spectroscopy to observe, in real time, the chemistry behind those laser-generated shocks (McGrane et al. 2003).

We also have little understanding of how the fine-scale substructures and hotspots in the detonation reaction zone affect detonation initiation and propagation. Figure 4(a) shows a photomicrograph of the granular substructure of PBX 9501. Research on the complex, micromechanical, hydrodynamic interactions that develop when such a material is subjected to a shock wave is still in its infancy—see Figures 4(b) and 4(c).

Measuring Reaction-Zone Effects

Because the length of the effective reaction zone affects the sensitivity to initiation as well as the detonation speed and extinction rates, we would like to predict its size. Since we cannot predict the reaction scale *ab initio*, we have taken a more phenomenological approach. That is, we have performed macroscale continuum experiments to measure the effects of the reaction-zone length, and we have developed continuum theories and models that, when forced to match those measurements, allow us to infer the global reaction-zone lengths and reaction rates.

The experiments are done on samples whose dimensions run from a few to many centimeters. Some experiments subject the explosive sample to

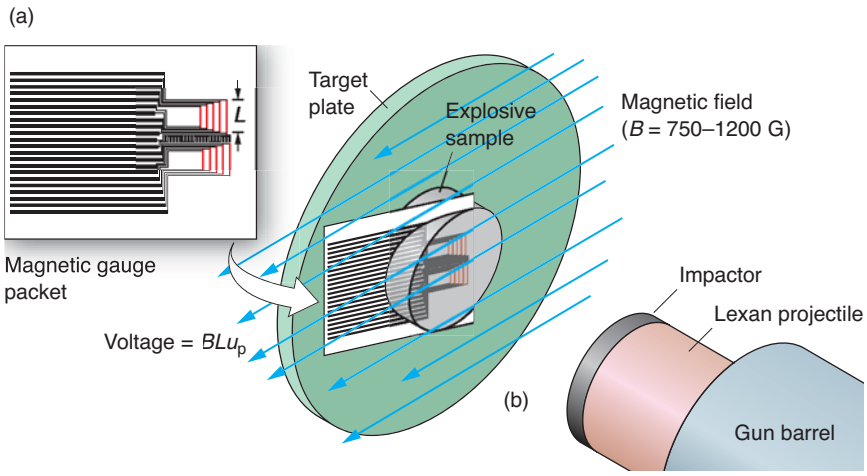

Figure 5. Magnetic Gauge Measurement of 1-D Detonation Flows
(a) A nested set of 10 magnetic gauges made of thin conducting wires is embedded obliquely relative to the faces of an explosive sample, and the sample is placed in a magnetic field of strength *B*. (b) The impact of a planar projectile initiates detonation. When the active elements in the gauge package, of length *L* and shown in red, are moved by the explosive flow, they cut the magnetic flux lines, thereby producing a voltage directly proportional to the velocity of the flow, u_p, at each gauge location. Thus, the 10 active elements track the history of 10 different particles in the explosive. The gauge package has a thickness of 60 μm and is capable of a time resolution of 20 ns (Sheffield et al. 1999).

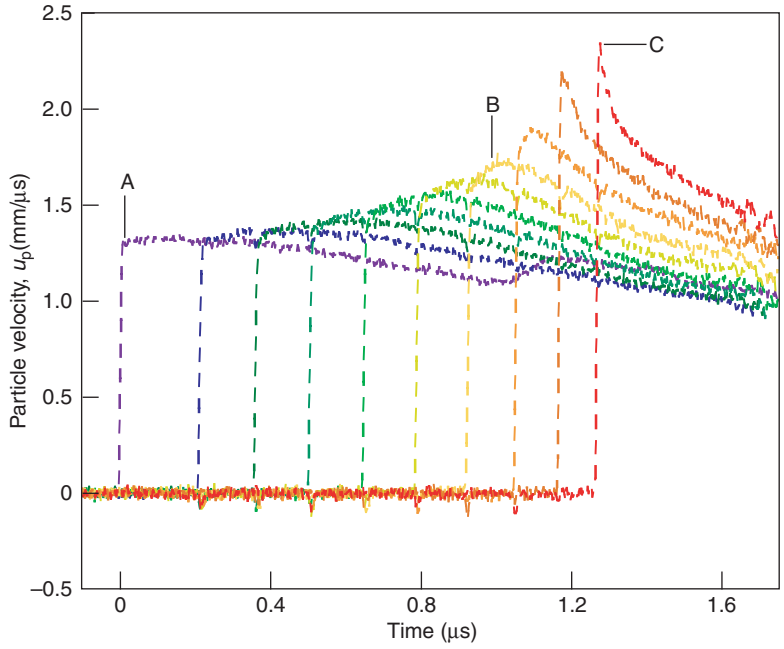

Figure 6. Magnetic Gauge Particle Histories for 1-D Detonation Flow
Shown here are the results from a magnetic gauge experiment on the insensitive high explosive PBX 9502. The input pressure was 0.135 Mbar. The experimental traces follow the transformation of a planar shock wave into a detonation. (Point A is the input state, point B indicates an interior velocity maximum, and point C is the ZND point. The shape change in the particle velocity profile (from an interior velocity maximum to a maximum at the shock) coincides with the first appearance of a choked flow condition, or sonic condition (Sheffield et al. 1998).

1-D detonation hydrodynamic flows (planar impacts in simple explosive geometries), whereas others generate and measure fully 3-D flows (resulting mostly from complex explosive geometries). Although the reaction-zone length can be quite short—about 0.01 millimeter for some of the sensitive explosives—its effects can be detected because detonation hydrodynamics tends to amplify any changes in initial or boundary conditions. (This property can be seen in Figure 1, where the transients occur over a distance of many reaction-zone lengths and later in Figure 10, where the overall displacement of the multidimensional detonation shock is measured in a number of reaction-zone lengths.) Still, the experiments must be capable of nanosecond time resolution in order to characterize the hydrodynamic response of these explosives.

In the high-resolution 1-D experiment shown in Figure 5, a nested set of 10 magnetic velocity gauges made of thin conducting wires is embedded obliquely, relative to the faces of an explosive sample, and the sample is placed in a magnetic field (Sheffield et al. 1999). A planar projectile impacts one of its faces as shown, and the quiescent sample begins to react and ultimately detonates. The active elements in the gauge package, shown in red, maintain their shape as they move with the explosive flow in the direction of the detonation front. As they move, they cut through the magnetic flux lines, producing a voltage directly proportional to the velocity of the flow at each gauge location. Thus, the 10 active elements track the history of 10 different particles in the explosive. The gauge package has a thickness of 60 micrometers and is capable of a time resolution of 20 nanoseconds. Note that, because the multiple-gauge package is mounted obliquely to the principal flow direction, the gauges farther upstream are not perturbed by those

downstream.

Figure 6 shows 10 particle-velocity histories, one from each magnetic gauge, for the insensitive high explosive PBX 9502 subjected to a planar impact with an initial pressure of 0.135 megabar (Sheffield et al. 1998). The series of particle histories (from left to right) reflects the transformation of a planar shock wave supported by the energy from the projectile impact into detonation supported by the energy release in the explosive. The gauges nearest the impact surface (leftmost trace) record the progress of what is essentially an inert shock wave passing through the explosive, whereas the later gauges show what, at least at first glance, resembles a classical ZND detonation structure (a shock followed by decreasing particle velocity through the reaction zone, as in Figure 1). The shock speed, also recorded in these experiments, shows an initial constant-velocity shock that then accelerates rapidly to a new, higher speed (approaching the detonation speed). The point of maximum acceleration, called the point of detonation formation, coincides with the shape change in the particle-velocity profile and the first appearance of the condition of choked flow (sonic condition).

Modeling the Detonation Reaction Zone

To infer more specific information on the global heat-release rate and the detonation reaction-zone length from these and other hydrodynamic measurements, we must model the detonation process. We first discuss the standard modeling paradigm. By comparing its predictions with experiment, we show that it can model 1-D flows fairly well but has serious shortcomings when applied to 3-D flows. Finally, we show how we have altered the standard paradigm to create the DSD model that not only solves some of those shortcomings but also is computationally efficient and suitable for use in the ASCI codes.

In the standard models, a detonating explosive is described as a continuous medium that obeys the conservation of mass, momentum, and energy for an Euler fluid:

$$\frac{\partial \rho}{\partial t} + \nabla \cdot (\rho \boldsymbol{u}) = 0 \ , \tag{1}$$

$$\frac{\partial \rho \boldsymbol{u}}{\partial t} + \nabla \cdot (\rho \boldsymbol{u}\boldsymbol{u} + \boldsymbol{I}P) = 0 \ , \tag{2}$$

$$\frac{\partial \rho e}{\partial t} + \nabla \cdot \left[(\rho e + P)\boldsymbol{u} \right] = 0 \ , \tag{3}$$

where $\boldsymbol{I}$ is the identity matrix, $\boldsymbol{u}$ is the particle velocity in the laboratory frame, P is the pressure, $\rho = v^{-1}$ is the density, $e = E + \boldsymbol{u} \cdot \boldsymbol{u}/2$, and E is the specific internal energy of the reacting explosive as a function of density and pressure. The energy E as a function of pressure and specific volume, $E(P, v)$, is the particular constitutive law (a law determined solely by the intrinsic properties of the material) that we introduced earlier as the mechanical EOS, and it must be provided as input to the fluid equations.

Because the much used Chapman-Jouguet theory requires as input a mechanical EOS of the form, $E_g(P_g, v_g)$, where the subscript g denotes detonation product gas, some realizations of $E_g(P_g, v_g)$ are available. To obtain an analogous expression for unreacted solid explosive, $E_s(P_s, v_s)$, one can start from a simple Mie-Gruneisen EOS and calibrate it to replicate the measured jump-off (shock state) value of the particle velocity seen with the magnetic gauges (as in Figure 6) and the measured shock velocity. To construct a mechanical EOS for the reacting mixture of solid and gas, one typically assumes pressure equilibrium between the solid and the gas, $P = P_s = P_g$. Then, to interpolate between the equations of state for the gas and the solid, one assumes that the internal energy and density of the mixture are given by

$$E(P, v, \lambda) = (1 - \lambda) E_s(P, v_s) + \lambda E_g(P, v_g) \ , \tag{4}$$

and

$$1/\rho = (1 - \lambda) v_s + \lambda v_g \ , \tag{5}$$

where λ is the mass fraction of reaction product gases.

Closure is brought to this system of equations, namely, Equations (1)–(5), with two additional assumptions. First, by extending the mechanical equations of state to include a simple temperature dependence and then assuming that the temperatures of the two phases are equal, $T = T_s = T_g$, one can relate v_s and v_g and thereby eliminate these intermediate variables from the problem. Second, one assumes that the rate of conversion of solid to gas in the reaction zone is given by an average, effective global heat-release rate law of the form

$$\frac{\partial \lambda}{\partial t} + \boldsymbol{u} \cdot \nabla \lambda = R(P, v, \lambda) \ , \tag{6}$$

where the heat-release rate function $R(P, v, \lambda)$ is constituted so that the gauge data in Figure 6 and other rate-dependent data are reproduced.

The Lee-Tarver Ignition and Growth model (Tarver and McGuire 2002) is an example of the standard modeling paradigm. It uses an empirical EOS for each of the components and takes appropriate account of the detonation energy in the unreacted explosive. It also uses an empirical form for the global heat-release rate function in Equation (6). The sets of constants for the equations of state of each explosive have been calibrated to a suite of hydrodynamic experiments performed on each explosive (see the box on the opposite page).

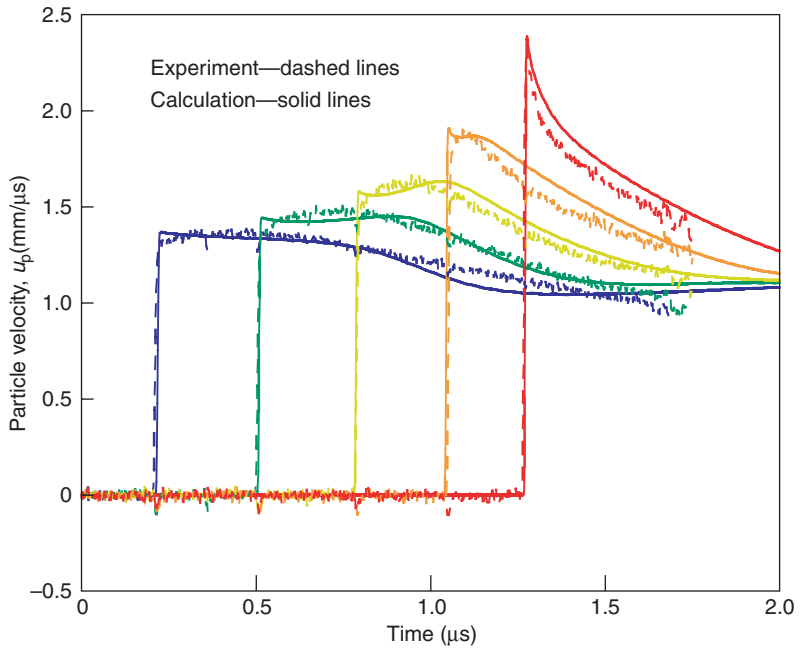

Figure 7. Comparison of Model with Experiment for 1-D Detonation
Predictions of the standard modeling paradigm are compared with the measured particle histories for PBX 9502 shown in Figure 6. The calculations were done using the Lee-Tarver EOS and a recalibrated rate law. The computing mesh had a minimum of 1000 computational zones in the reaction zone. The agreement is reasonably good, but there are noticeable discrepancies.

EOS and Rate Law for the Ignition and Growth Model

The empirical Jones-Wilkins-Lee forms are used for both the solid (i = s) and the gas (i = g)

EOS
$$T = \frac{V_i}{\omega_i C_{Vi}}\left\{P - A_i \exp(-R_{1i}V_i) - B_i \exp(-R_{2i}V_i)\right\} ,$$

where $V_i = \rho_0/\rho_i$ and ω_i, C_{Vi}, A_i, B_i, R_{1i}, and R_{2i} are calibration parameters.

The internal energy is solved for using the thermodynamic constraint

$$\left\{P - \rho^2\left(\frac{\partial e}{\partial \rho}\right)_P\right\}\left(\frac{\partial T}{\partial P}\right)_\rho + \rho^2\left(\frac{\partial e}{\partial P}\right)_\rho\left(\frac{\partial T}{\partial \rho}\right)_P = T \quad .$$

The heat-release rate law is given by

Rate Law
$$R(P,v,\lambda) = IH\left(\lambda_1^* - \lambda\right)(1-\lambda)(1/V - 1 - a)^7 + G_1 H\left(\lambda_2^* - \lambda\right)(1-\lambda)\lambda^{0.111}P + G_2 H\left(\lambda - \lambda_3^*\right)(1-\lambda)\lambda P^3 ,$$

where $0 \le \lambda \le 1$ describes the progress of the global heat-release reaction ($\lambda = 0$, is unreacted, and $\lambda = 1$ is fully reacted), $H(\lambda_i^* - \lambda)$ is the unit step function, and I, a, G_1, G_2, and λ_i^* are parameters.

The authors and Ashwani Kapila of Rensselaer Politechnic Institute (private communication—2003), used the Lee-Tarver Ignition and Growth model to predict the results of the magnetic gauge experiment for PBX 9502 shown in Figure 6. To solve Equations (1)–(6), these authors and others have developed solution algorithms and adaptive mesh refinement codes (Aslam 2003, Fedkiw et al. 1999,Quirk 1998, Henshaw and Schwendeman 2003). Here, we used a minimum of 1000 computational zones to model the reaction zone. Figure 7 compares the simulation results with the experimental data for PBX 9502. The wave profile that develops far from the initiating piston surface (that is, to the far right) clearly shows a nearly steady-state reaction zone. We see that this phenomenological model—a simple homogeneous fluid model with a global reaction rate—mimics a 1-D experiment reasonably well. However, it does not describe the complicated interaction between hydrodynamic hotspots and fundamental chemical processes, an interaction that produces the heat release rate in effective, global, heterogeneous explosives.

Application of Standard Models to Multidimensional Flows

The class of models just described has been applied to problems with fully 3-D geometries, but our studies show that the solutions contain features that are unsatisfactory for use in real performance codes. As an example, we consider the propagation of a detonation wave in a stack of right-circular cylinders of explosive—see Figure 8(a). The object is to predict the progress of detonation as it diffracts from a smaller to a larger coaxial cylinder. We simulated this experiment with a model similar to that described above but with a simpler EOS and a simpler rate law

for the reaction zone. The EOS for the unreacted and reacted explosive is obtained by setting $A_i = B_i = 0$ and $\omega_s = \omega_g = 2$ and by simplifying the rate law to

$$R(P, v, \lambda) = kP^n(1-\lambda)^\mu \ , \qquad (7)$$

where k is a constant and μ is set to $\mu = 1/2$. All constants were selected to mimic the condensed-phase explosive PBX 9502. In the experiment, the explosive is embedded in a low-density plastic. The plastic does not affect the flow in the reaction zone; rather the explosive behaves as it would if it were totally unconfined (floating in free space). We simulated the experiment using the Amrita (Quirk 1998) computational environment, which provides adaptive mesh refinement, simulation scheduling, and documentation of the results. We also used the Ghost Fluid interface-tracking algorithm (Fedkiw et al. 1999) to keep a sharp interface between the explosive and the confining inert plastic and a Lax-Friedrichs solver to update the flow.

Figures 8(b) and 8(c) are composites. Each shows two solutions for the pressure—one before and one after the detonation passes into the wider (acceptor) section of the explosive. These two figures differ in that they show solutions for two different energy-release rate functions R—Equation (7)—proportional to the square of the pressure, $n = 2$, and the cube of the pressure, $n = 3$, respectively. The top and bottom halves of each figure show results for different resolutions in the steady-state ZND reaction zone, 72 and 18 points, respectively, for the $n = 2$ solution, and 18 and 9 points, respectively, for the $n = 3$ solution. For both rate laws, the location of the detonation front depends significantly on numerical resolution. Also, for the $n = 3$ rate law, the detonation is highly unstable: There are very large pres-

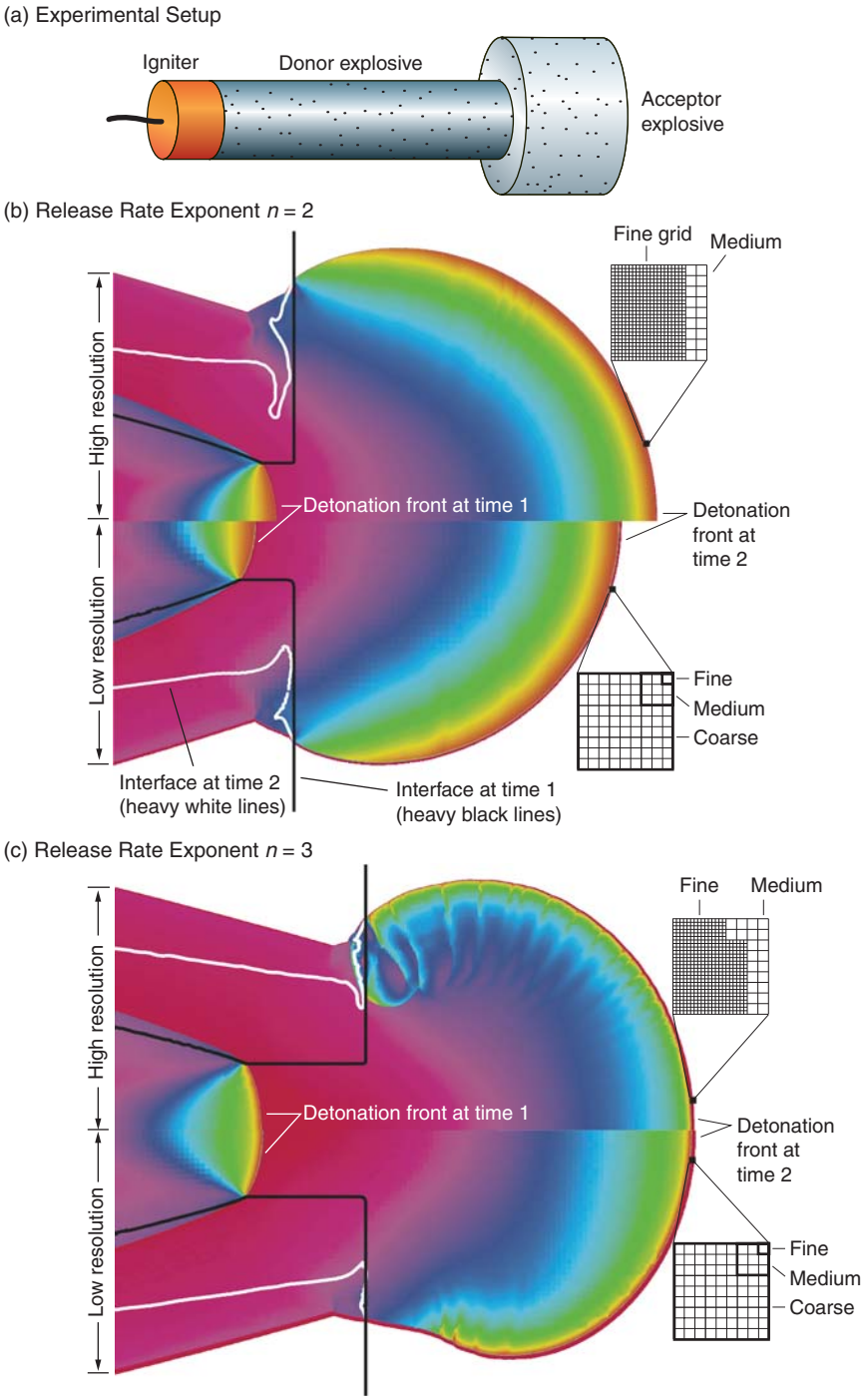

Figure 8. Standard Modeling of Detonation in 3-D Geometries
In (a) we show the setup for detonation wave propagation in a stack of right-circular cylinders, and in (b) and (c) we show the results from the standard modeling paradigm with different energy-release rate laws, $n = 2$ and $n = 3$ with $\mu = 1/2$ in Equation (7). In each case, top and bottom figures display the results for different resolutions: 72 and 18 points in the reaction zone for $n = 2$ and 18 and 9 points in the reaction zone for $n = 3$, respectively. In both cases, the results change markedly with increasing resolution. Also, with the more pressure-sensitive rate law, $n = 3$, the reaction zone shows high-frequency structure that is an artifact of this modeling paradigm for heterogeneous explosives.

sure and high-frequency structures in the acceptor explosive (wider section), and the details of the instability are very much resolution dependent.

Short et al. (2003) have analyzed the stability of the classical, steady-state ZND reaction-zone structure to small, multi-dimensional disturbances and shown that it is unstable to even small perturbations whenever n is greater than 2.1675 for the model that we have described here. Figure 9 shows the results of this stability analysis. Also, the addition of a nozzling term to Equation (3) (that term mimics the energy loss from the reaction zone because of multidimensional flow effects) leads to a further destabilization of the reaction zone to 1-D disturbances. (Note: The high-resolution $n = 2$ simulation also shows some signs of instability.) The root of this instability can be understood with the following argument. Detonation in this homogeneous-fluid model is a balance between shock-initiated energy-releasing reactions and the acoustic transport of that energy to support the shock. When a pressure perturbation in the reaction zone affects the reaction rate much more than it does the sound speed, then small pressure fluctuations can disrupt the balance between energy liberation and transport, and instability can be the result.

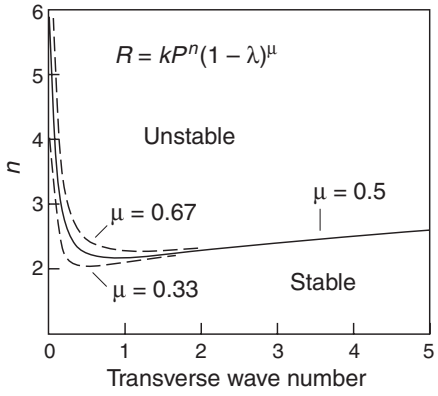

Figure 9. Stability Analysis Results for the Standard Detonation Modeling Paradigm
The vertical axis is the pressure exponent of the heat-release rate *R*, and the horizontal axis is the wave number of the perturbing transverse disturbance. For any state above the curve, the ZND detonation is unstable. For $\mu = 0.5$, a ZND detonation is unstable to two-dimensional disturbances whenever $n > 2.1675$.

Problems with the Reaction-Zone Modeling Paradigm

Both the dependence on numerical resolution and the appearance of the high-frequency structure in the acceptor region of the explosive represent a significant problem for this modeling paradigm. In independent studies of this simple model for the $n = 2$ case, we have shown that to predict the detonation speed in the donor section to within 10 m/s requires 50 or more points in the ZND reaction zone. (Aslam et al. 1998). This number translates into a very computationally intensive problem for typical 3-D engineering scale problems, where the reaction-zone length is very much shorter than the dimension of the explosive piece. At any instant, about 10^{10} relatively small computational nodes would be needed in the reaction zone, and the computational time on a large parallel processing computer would be about 100 days. Second, the high-frequency, acoustically based transverse wave structure is an artifact of this simple homogeneous-fluid model and is not observed in our heterogeneous explosives. The substructure associated with the granular structure of real heterogeneous explosives derives from the material particles, not acoustic waves. In fact, the granularity inhibits the formation of large transverse acoustic waves. Thus, although the simple homogeneous-fluid model reproduces reasonably well the leading-order features of detonation, such as the ZND structure, it fails to describe higher-order features of real heterogeneous explosives.

DSD, a Subscale Model of Detonation

We have championed an approach to the performance problem that is philosophically different from the standard paradigm just described (Aslam et al. 1996). In the DSD approach, we exploit the fact that the explosive pieces of engineering interest are large compared with the reaction-zone length and substitute a subscale model for the detailed model of the reaction zone. To construct this subscale model, we consider how the detonation reaction zone is influenced by weak curvature of the shock front and derive a constraint equation relating the speed of the detonation front to the shape of that front. We then derive a boundary condition on that equation that relates edge effects to the detonation wave shape. Thus, on the scale of the explosive, the reaction zone becomes a front, a discontinuity, separating fresh from burnt explosive. In this way, DSD focuses on the two primary goals of the performance problem: accurate prediction of (1) the local detonation speed and detonation arrival times in a weapons simulation and (2) the P-v (pressure-volume) work that the high-pressure detonation products can perform on the inert materials with which the explosive is in contact. As we will see, this approach also filters out the high-frequency features and vastly reduces the computational requirements by comparison with the standard modeling paradigm described above.

Figure 10 shows a detailed view of the reaction zone and shock front, with unburnt explosive above and burnt explosive below. The reaction-zone length is short compared with the explosive charge dimension, L. In place of Cartesian coordinates, we use coordinates that are attached to the shock surface (see the upper inset in Figure 10). The constant η is the dis-

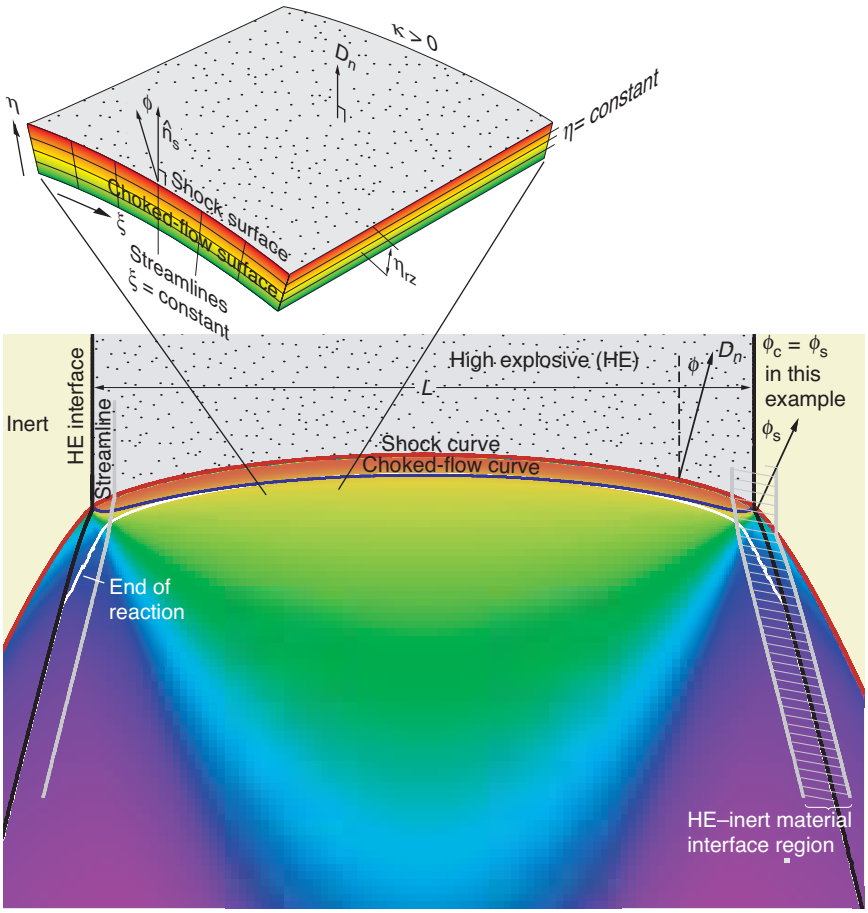

Figure 10. Multidimensional Reaction Zone and the DSD Shock-Attached Coordinates

A multidimensional reaction zone in a cylindrical detonating explosive (gray) is weakly confined at its edges by a low-density inert material (yellow). As shown, the reaction zone is typically short compared with the dimension of the explosive charge, *L*. The upper inset depicts a segment of the 3-D reaction zone with the intrinsic shock-attached coordinates used in DSD analysis. In the DSD limit, the ratio of the reaction-zone thickness to the scale of the explosive charge is very, very small, $\eta_{rz}/L = O(\varepsilon) << 1$, and a subscale front model takes the place of the detailed reaction-zone model. The crosshatched area, approximately the width of the reaction zone and straddling the explosive–inert material interface, defines the region where an analysis of the boundary region is performed. As explained in the text, that analysis leads to boundary conditions for the subscale model.

tance through the reaction zone normal to the shock surface, and ξ is the distance along the shock measured from the centerline of the explosive. Thus, curves of constant η are parallel to the shock, and the lines of constant ξ are in the direction of the local normal to the shock surface. Because the features of interest are on the scale of the explosive, we define a dimensionless scale, $\varepsilon = \eta_{rz}/L << 1$, where η_{rz} is the scale of the detonation reaction-zone length. This scale aids in the derivation of the subscale model.

DSD assumes that the detonation reaction zone departs from its 1-D (planar) steady-state ZND form by a small amount. That small departure is determined by both the size of the shock curvature κ measured in units of the reaction-zone length scale η_{rz}, ($\eta_{rz}\kappa = O(\varepsilon) << 1$) and the departure of D_n, the detonation speed in the direction of the shock normal vector, from D_{CJ}, the detonation speed for a 1-D steady-state wave. The relevant scaled detonation speed is $(D_n/D_{CJ} - 1) = \mathcal{D} = \varepsilon\mathcal{D}^{\sim}$

To construct an asymptotic solution—a solution in the limit that $\varepsilon << 1$ —for the multidimensional detonation reaction-zone flow, we first introduce into the standard detonation model, Equations (1)–(3) and (6), the following slowly changing, scaled, independent variables:

$$\tilde{t} = \varepsilon t \ , \tilde{\xi} = \varepsilon^{1/2}\xi \ , \phi = \varepsilon^{1/2}\tilde{\phi} \ , \qquad (8)$$

where ϕ is the shock normal angle defined in Figure 10. We then expand the solution vector $Y = (\rho, u_\eta P)^T$ as

$$Y = Y^{(0)} + \varepsilon Y^{(1)} + \varepsilon^2 Y^{(2)} + \ \ldots \ , \qquad (9)$$

$$u_\xi = \varepsilon^{3/2} u_\xi^{3/2} + \ \ldots \ , \qquad (10)$$

The leading order term in the solution vector (designated with a superscript 0) represents the 1-D ZND solution, whereas the terms proportional to powers of ε bring in the effects of multidimensionality and time dependence. A compatibility constraint emerges on the solution that forces a relationship between the shock curvature κ and various derivatives of the scaled detonation speed $\mathcal{D}$

$$\mathcal{F}(\mathcal{D}) = \kappa + \mathcal{A}(\mathcal{D})\frac{D\mathcal{D}}{Dt} - \mathcal{B}(\mathcal{D})\frac{\partial^2 \mathcal{D}}{\partial \xi^2} + \ldots \ , \qquad (11)$$

where $\mathcal{F}(\mathcal{D})$ is a decreasing function of $\mathcal{D}$ with $\mathcal{F}(0) = 0$, $\mathcal{A}(\mathcal{D}) > 0$ and $\mathcal{B}(\mathcal{D}) > 0$. A term-by-term examination of the right-hand side of this equation shows that (1) increasing κ (shock curvature) slows the detonation wave, (2) the acceleration term $\mathcal{A}(\mathcal{D})(D\mathcal{D}/Dt)$ acts like inertia and resists changes in the front speed and

shape, and (3) the dissipative term $\mathcal{B}(\mathcal{D})(\partial^2\mathcal{D}/\partial\xi^2)$ damps high frequencies and thus the formation of kinks on the wave front. The dispersion relation for the linearized form of Equation (11)

$$\omega = -ik^2\left(\mathcal{B}/2\mathcal{A}\right) \pm \sqrt{k^2/\mathcal{A} - k^4\left(\mathcal{B}/2\mathcal{A}\right)^2} \qquad (12)$$

reveals that, at low transverse frequencies (small values of the wave number k), Equation (11) predicts dissipative, transverse waves moving along the front. On the other hand, at high transverse frequencies (large k), Equation (11) is purely dissipative. Thus, by adopting the scaled variables of Equation (8), high-frequency features such as kinks on the front will not form.

Thus, on the scale of the explosive piece, the detonation reaction zone looks like a discontinuity separating fresh and burnt explosive. Moreover, this discontinuity occurs along a surface that propagates according to the dynamics given by Equation (11), which can be viewed as an intrinsic detonation propagation law for an explosive. It is important to recognize that the forms of the coefficient functions $\mathcal{F}(\mathcal{D})$, $\mathcal{A}(\mathcal{D})$, and $\mathcal{B}(\mathcal{D})$ depend on the material description of the explosive (the EOS and the global heat-release rate).

In addition to specifying a propagation law such as Equation (11), we need to prescribe a boundary condition on the front, where the front meets the edge of the explosive piece (see the right portion of Figure 10). Just as we constructed a subscale model to mimic the effects of the reaction zone on the front motion, we construct a subscale model to mimic the effect of confinement by adjacent inert materials on the detonation speed. Roughly speaking, the more compliant the inert materials, the greater the deflection of explosive streamlines and shock angle ϕ and the greater the pressure drop. A boundary layer analysis performed within a distance of one reaction-zone length on either side of the explosive–inert material interface reveals (see cross-hatched region) that this interaction establishes a unique shock-edge angle, ϕ_c, which is a function of the explosive and inert material pair considered. That angle serves as a boundary condition for Equation (11). The weaker the confinement, the greater the value of ϕ_c, up to the point where the lateral expansion of the detonation products becomes choked (the development of a sonic state behind the shock, as shown in Figure 10), halting any further drop in pressure at the shock. This phenomenon occurs at a value of ϕ called the sonic angle, ϕ_s, which depends solely on the properties of the explosive and is about 45° for our explosives (Aslam and Bdzil 2002, Bdzil 1981).

DSD Calibration and Propagation of Detonation Front

To validate the DSD approach, we used it to compute the detonation front shapes for the rate law of Equation (7) and compared the DSD results with numerical results from the standard paradigm, Equations (1)–(3), (6), and (7). The good agreement validates the DSD approach, at least for n <2.1675, for which the standard approach is fairly accurate (Aslam et al. 1998). Although we could have derived a detonation propagation law directly from a calibrated shock-initiation model, such as the Lee-Tarver Ignition and Growth model, we chose, instead, to derive Equation (11) more generically and calibrate it from experimental data on multidimensional detonation. In that way, we bypassed artifacts of the homogeneous-fluid model paradigm and built in features faithful to real, heterogeneous explosives but not easily modeled with the standard paradigm.

Calibration data are often obtained from measurements of the detonation speed and front curvature in explosive cylinders of various sizes (see Figure 11). For explosives such as PBX 9502, those data can be fit reasonably well with just the leading term in the propagation law of Equation (11):

$$\kappa = \mathcal{F}(\mathcal{D}) \ , \qquad (13)$$

which specifies a simple relationship between the detonation speed and the detonation shock-front curvature. The propagation law so obtained for PBX 9502 predicts that the shock-normal detonation speed decreases substantially with increasing shock-front curvature (see Figure 12). Figure 13(a) shows a DSD prediction for the detonation front shape at initiation and two later times as the detonation propagates through an arc of PBX 9502. Figure 13(b), a top-down view, shows the DSD solution lagging behind the simple constant-velocity CJ solution. The significant differences between these two argue for the importance of

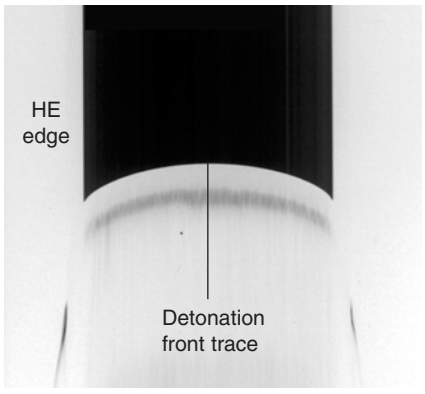

Figure 11. Detonation Front Measurement in a Cylinder of Explosive

This image, taken by a streak camera, shows the detonation front arrival time vs radius at the planar face of the explosive cylinder (Hill 1998).

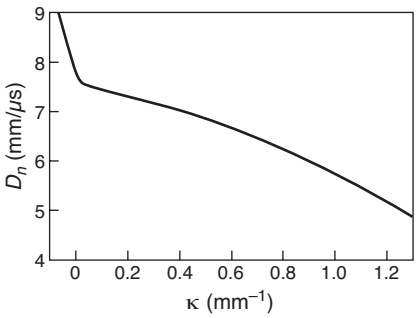

Figure 12. DSD Propagation Law for PBX 9502 at 25°C

The DSD propagation law predicts that detonation speed normal to the shock D_n decreases substantially with increasing shock-front curvature κ.

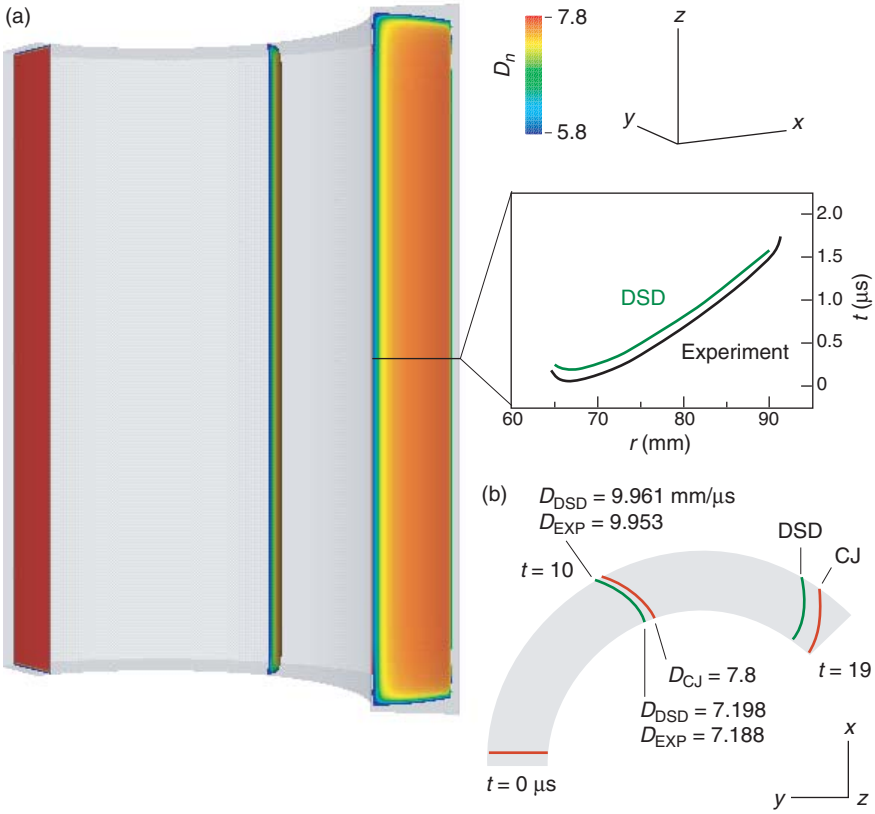

Figure 13. DSD Detonation through an Arc of PBX 9502

(a) The 3-D composite image shows the progress of the DSD front through an explosive arc. Each detonation front is colored by the local instantaneous normal detonation speed. The slowing of the detonation near the edges is apparent by the change in color from red to green. Shown in the inset are plots of the DSD (green) and experimental (black) times of arrival of the detonation front along the midline of the planar edge of the arc (measured in units of the cylinder radius). The resulting curves show the similarity between the DSD and measured wave-front shapes. The DSD and experimental plots are set off to display results. (b) This top-down view shows the intersection of the DSD and CJ fronts with a plane passing through the middle of the arc. The DSD detonation speed slows down by 10% relative to its initial value, whereas the CJ detonation speed is constant. Consequently, there is a growing separation of DSD and CJ fronts. The phase velocities of the DSD wave along the inner and outer surfaces of the arc agree well with the experimental values.

including reaction-zone effects. The DSD shapes and velocities are in very good agreement with experiment

To obtain the DSD solution shown in Figure 13, we start from the front propagation law and edge boundary conditions and use level-set methods to compute the propagation of the front. These methods work by embedding the detonation front in a level-set function, Ψ, and then evolving this function according to

$$\partial\psi/\partial t + D_n|\nabla\psi| = 0 \quad . \qquad (14)$$

By our definition, the level surface $\psi = 0$ corresponds to the detonation front initially and at any subsequent time. We compute the actual detonation front by finding the $\psi = 0$ contour. The level-set methodology offers significant computational advantages because it enables easy handling of complex explosive topologies and detonation interactions.

This past year, we have developed a first-order accurate, 3-D computational algorithm that uses the level-set method and that runs on parallel computing platforms. Results from that method are shown in Figure 14, which displays a detonation initiated simultaneously at the ends of two symmetrical legs and propagating through a piece of PBX 9502 with complex geometry. The detonation fronts are shown at four different times. The shape of the explosive, two protruding legs on one side and a cylindrical hole on the other, forces the detonation fronts to merge ($t = t_3$) and then bifurcate ($t = t_4$). Merging and bifurcation of different detonation fronts are automatically treated with the level-set-based DSD approach. For comparison, the CJ wave is also shown (as ahead) in the last snapshot ($t = t_4$).

New Modeling Paradigms for Detonation Reaction Zones

The methods just described represent the state of the art in detonation modeling for engineering applications. In closing, we outline our vision for the future.

The modeling paradigm represented

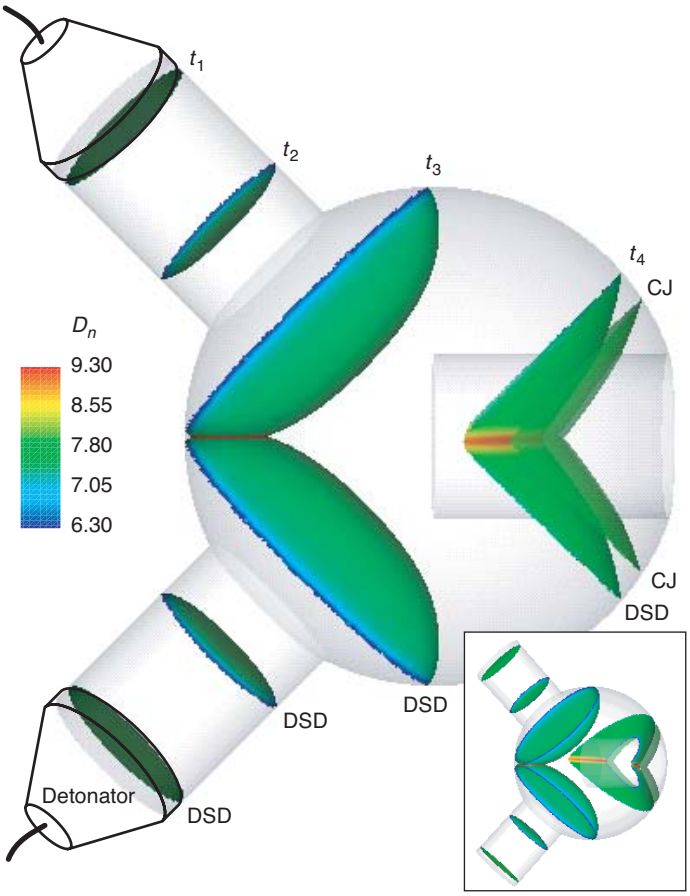

Figure 14. A 3-D DSD Calculation

This example shows how DSD can handle the merging of separated detonation fronts, the acceleration of the detonation in regions where the fronts converge, and the bifurcation of the detonation wave around obstacles. Detonation starts in the two legs (left side of the figure) and progresses toward the cylindrical hole on the right. Four snapshots show the progress of the detonation waves through the sample, and the DSD and CJ calculations are compared on the fourth snapshot. The detonation front is colored with the local value of the detonation speed. The inset shows an oblique view.

by Equations (1)–(6) has serious shortcomings. Principally, such a continuum model does not include any phenomenon that might be important for heterogeneous materials, such as scattering or dispersion of acoustic waves and dissipation of energy from the reaction-zone scale to the subreaction-zone scales of the hotspots. Current models are effective for homogeneous explosives. As we better understand the details of the hotspots and reaction chemistry under detonation conditions, we will need to develop better continuum models. If subnano-scale measurements support our current view that the chemical reactions important in detonation are extremely state sensitive, then very short scale regions where the hotspot temperatures are most extreme will have a disproportionate effect toward accelerating the reaction chemistry (Bdzil et al. 1999, Menikoff and Kober 1999). These would be subgrain scales, related more to details of the grain shape than the grain volume (Figure 4 shows how complex this substructure can be). The notion of doing numerically resolved meso-scale simulations of detonation in granular explosives and then somehow averaging those results to develop appropriate continuum-level engineering models seems to be many years away.

Given our lack of detailed information about the relationship between the geometry of explosive grains and the constitutive properties of our materials (including, for example, heat conductivity) under detonation conditions, a more realistic midterm goal is to develop subscale models for the reaction zone in which behaviors on the grain and subgrain scales are parameterized in terms of longer wavelength variables. We are working to develop rational asymptotic models that indicate not only how the explosives' global heat-release rate should be modeled but also how the presence of granularity and hotspots in these materials affects the basic modeling structure—that is, what modifications need to be made to Equations (1)–(6). For example, significant density variations in a material on a short-wavelength scale will appear on the long-wavelength continuum scale as dispersion terms added to the basic conservation laws—refer to Equations (1)–(3). The presence of such terms could be expected to scatter acoustic waves and inhibit the detonation modeling instabilities that we have observed in our homogeneous-explosive models. Whatever improved modeling paradigms are developed for the continuum response of heterogeneous explosives, we expect that, for the foreseeable future, models will have to be calibrated to experiments if they are to make the accurate predictions of detonation propagation necessary for weapons simulations. ■

Further Reading

Aslam, T. D. 2003. A Level Set Algorithm for Tracking Discontinuities in Hyperbolic Conservation Laws II: Systems of Equations (to be published in *J. Sci. Comput*. **19** (1–3), December 2003).

Aslam, T. D., and J. B. Bdzil. 2002. "Numerical and Theoretical Investigations on Detonation-Inert Confinement Interaction." Twelfth Symposium (Int.) on Detonation, San Diego, California, August 11–16, 2002. Los Alamos National Laboratory document LA-UR-01-4664 (to be published in *Proceedings—Twelfth International Detonation Symposium*). [Online]: http://www.sainc.com/onr/detsymp/technicalProgram.htm

Aslam, T. D., J. B. Bdzil, and L. G. Hill. 2000. "Extensions to DSD Theory: Analysis of PBX 9502 Rate Stick Data." In *Proceedings—Eleventh International Detonation Symposium,* ONR 33300-5, pp. 21–29. Arlington, Virginia: Office of Naval Research.

Aslam, T. D., J. B. Bdzil, and D. S. Stewart. 1996. Level Set Methods Applied to Modeling Detonation Shock Dynamics. *J. Comput. Phys*. **126** (2): 390.

Bdzil, J. B. 1981. Steady-State Two-Dimensional Detonation. *J. Fluid Mech.* **108**: 195.

Bdzil, J. B., R. Menikoff, S. F. Son, A. K. Kapila, and D. S. Stewart. 1999. Two-Phase Modeling of Deflagration-to-Detonation Transition in Granular Materials: A Critical Examination of Modeling Issues. *Phys. Fluids* **11** (2): 378.

Campbell, A. W., and J. R. Travis. 1985. "Shock Desensitization of PBX-9404 and Composition B-3." In *Proceedings—Eighth International Detonation Symposium,* J. M. Short, Ed., pp. 1057–1068. Naval Surface Weapons Center, NSWC MP 86-194.

Fedkiw, R. P., T. Aslam, B. Merriman, and S. Osher. 1999. A Non-Oscillatory Eulerian Approach to Interfaces in Multimaterial Flows (the Ghost Fluid Method). *J. Comput. Phys*. **152** (2): 457.

Henshaw, W. D., and D. W. Schwendeman. 2003. "An Adaptive Numerical Scheme for High-Speed Reactive Flow on Overlapping Grids." Lawrence Livermore National Laboratory preprint UCRL-JC-151574 (submitted to *J. Comput. Phys.*).

Hill, L. G. 2002. "Development of the LANL Sandwich Test." In *Shock Compression of Condensed Matter—2001: Proceedings of the Conference of the American Physical Society, Topical Group on Shock Compression of Condensed Matter*, M. D. Furnish, Y. Horie, and N. N. Thadhani, Eds. Vol. 620 (1), pp. 149–152. Secaucus, New Jersey: Springer-Verlag.

Hill, L. G., Bdzil, J. B., and T. D. Aslam.2000. "Front Curvature Rate Stick Measurements and Detonation Shock Dynamics Calibration for PBX9502 over a Wide Temperature Range." In *Proceedings—Eleventh International Detonation Symposium,* ONR 33300-5, pp. 1029–1037. Arlington, Virginia: Office of Naval Research.

McGrane, S. D., D. S. Moore, and D. J. Funk. 2003. Sub-Picosecond Shock Interferometry of Transparent Thin Films. *J. Appl. Phys.* **93** (9): 5063.

Menikoff, R., and E. M. Kober. 1999. "Compaction Waves in Granular HMX," Los Alamos National Laboratory report LA-13546-MS.

Quirk, J. J. 1998. AMRITA: "A Computational Facility (for CFD Modeling)." In 29th Computational Fluid Dynamics, von Karman Institute Lecture Series. ISSN 0377-8312.

Shaw, M. S. 2002. "Direct Simulation of Detonation Products Equation of State by a Composite Monte Carlo Method," Twelfth Symposium (Int.) on Detonation, San Diego, California, August 11–16, 2002 (to be published in *Proceedings—Twelfth International Detonation Symposium*). [Online]:http://www.sainc.com/onr/detsymp/technicalProgram.ht

Sheffield, S. A., R. L. Gustavsen, and R. R. Alcon. 2000. "In Situ Magnetic Gauging Technique Used at LANL—Method and Shock Information Obtained." In *Shock Compression of Condensed Matter—1999, AIP Conference Proceedings*, M. D. Furnish, L. C. Chhabildas, and R. S. Hixson, Eds., Vol. 505, p. 1043. Secaucus, New Jersey: Springer-Verlag.

Sheffield, S. A., R. L. Gustavsen, L. G. Hill, and R. R. Alcon. 2000. "Electromagnetic Gauge Measurements of Shock Initiating PBX9501 and PBX9502 Explosives." In *Proceedings—Eleventh International Detonation Symposium,* ONR 33300-5, pp. 451–458. Arlington, Virginia: Office of Naval Research.

Short, M., J. B. Bdzil, G. J. Sharpe, and I. Anguelova. Detonation Stability for a Condensed Phase Reaction Model with a Variable Reaction Order (submitted to *Combust. Theory Modell.*).

Skidmore, C. B., D. S. Phillips, and N. B. Crane. 1997. Microscopical Examination of Plastic-Bonded Explosives. *Microscope* **45** (4): 127.

Tarver, C., and E. McGuire. 2002. "Reactive Flow Modeling of the Interaction of TATB Detonation Waves with Inert Materials." Twelfth Symposium (Int.) on Detonation, San Diego, California, August 11–16, 2002 (to be published in *Proceedings—Twelfth International Detonation Symposium*). [Online]: http://www.sainc.com/onr/detsymp/technicalProgram.htm

Watt, S. D., and G. J. Sharpe. One-Dimensional Linear Stability of Curved Detonations (submitted to *Proc. R. Soc. Lond., Ser. A*).

For further information, contact Scott Watson (505) 667-8054 (jbb@lanl.gov).